Eur Biophys J (2005) 34: 127–143
DOI 10.1007/s00249-004-0436-x

ARTICLE

**Bálint Rubovszky · Péter Hajdú · Zoltán Krasznai
Rezsõ Gáspár Jr. · Thomas A. Waldmann
Sándor Damjanovich · László Bene**

Detection of channel proximity by nanoparticle-assisted delaying of toxin binding; a combined patch-clamp and flow cytometric energy transfer study

Published online: 16 September 2004

Abstract Gold nanoparticles of 30 nm diameter bound to cell-surface receptor major histocompatibility complex glycoproteins (MHCI and MHCII), interleukin-2 receptor α subunit (IL-2Rα), very late antigen-4 (VLA-4) integrin, transferrin receptor, and the receptor-type protein tyrosin phosphatase CD45 are shown by the patch-clamp technique to selectively modulate binding characteristics of Pi_2 toxin, an efficient blocker of $K_v1.3$ channels. After correlating the electrophysiological data with those on the underlying receptor clusters obtained by simultaneously conducted flow cytometric energy transfer measurements, the modulation was proved to be sensitive to the density and size of the receptor clusters, and to the locations of the receptors as well. Based on the observation that engagement of MHCII by a monoclonal antibody down-regulates channel current and based on the close nanometer-scale proximity of the MHCI and MHCII glycoproteins, an analogous experiment was carried out when gold nanoparticles bound to MHCI delayed down-regulation of the $K_v1.3$ current initiated by ligation of MHCII. Localization of $K_v1.3$ channels in the nanometer-scale vicinity of the MHC-containing lipid rafts is demonstrated for the first time. A method is proposed for detecting receptor–channel or receptor–receptor proximity by observing nanoparticle-induced increase in relaxation times following concentration jumps of ligands binding to channels or to receptors capable of regulating channel currents.

Keywords Interleukin receptor · Lipid raft · Major histocompatibility complex glycoproteins · Potassium channel · Very late antigen integrin

Abbreviations BSA: bovine serum albumin · CLSM: confocal laser scanning microscopy · Fab: Fab fragment · FCET: flow cytometric energy transfer · FRET: fluorescence resonance energy transfer · IL-2Rα: interleukin-2 receptor α subunit · mAb: monoclonal antibody · MHCI: major histocompatibility complex class I · MHCII: major histocompatibility complex class II · NSOM: near-field scanning optical microscopy · RAMIG: rabbit anti-mouse IgG · RD: reduction-in-dimensionality · TEM: transmission electron microscopy · TrfR: transferrin receptor · VLA-4: very late antigen-4

P. Hajdú · Z. Krasznai · R. Gáspár Jr. · S. Damjanovich
L. Bene (✉)
Department of Biophysics and Cell Biology,
Medical and Health Science Center,
University of Debrecen, Debrecen, Hungary
E-mail: bene@jaguar.dote.hu
Fax: +36-52-412623

B. Rubovszky · S. Damjanovich
Cell Biophysics Research Group,
Hungarian Academy of Sciences,
Nagyerdei krt. 98, PO Box 39, 4012
Debrecen, Hungary

T. A. Waldmann
Metabolism Branch, National Cancer Institute,
National Institutes of Health, Bethesda, MD, USA

Introduction

The existence and possible biological role of the cell-surface super-structures, mainly consisting of the major histocompatibility complex class I and class II (MHCI and MHCII) antigens, the interleukin-2 cytokine receptor (IL-2R) complex, and the intercellular adhesion molecule-1 (ICAM-1), have been recently described in a series of experiments (Bene et al. 1994; Mátyus et al. 1995; Szöllősi et al. 1996; Damjanovich et al. 1998, 1999; Vereb et al. 2000, 2003; Nagy et al. 2001; Bacsó et al. 2002; Matkó et al. 2002). The IL-2R activates STAT3, STAT5 and the *lck* family phosphotyrosines (e.g. $p56^{lck}$) through the Janus kinases (Jaks) (DiSanto 1997; Nelson and Willerford 1998) and plays an important role in the initiation of mitogen- or antigen-induced immune responses and in the activation induced cell death (AICD)

by activating the helper and cytotoxic T-lymphocytes in an autocrine fashion.

Interestingly, besides their established role in antigen presentation, MHCI and MHCII molecules have been recently described to have an active ''non-classical'' function in transmembrane signaling: they may even induce apoptosis or activate cells in a lineage- and differentiation state-dependent manner (Wade et al. 1993; Skov et al. 1997, 1998; Altomonte et al. 1999; Drénou et al. 1999). Moreover, the same tyrosine and serine kinases involved in the signaling of the IL-2 receptor were shown to be also coupled to MHC-triggered pathways as well (Wade et al. 1993; Skov et al. 1998; Huby et al. 1999). Furthermore, nanometer- and millimeter-scale hetero- and homo-associations of these molecules have been found to exhibit remarkable compositional similarity amongst the different cell lines examined (Bene et al. 1994; Szöllősiöllősi et al. 1996; Vereb et al. 2000, 2003; Nagy et al. 2001; Bacsó et al. 2002; Matkó et al. 2002). Ionic detergent-insoluble lipid microdomains (DIMs, DIGs, DRMs) rich in glycosphingolipid and cholesterol, also termed lipid rafts, were demonstrated to participate in maintaining these receptor clusters (Vereb et al. 2000, 2003; Matkó et al. 2002). Localizing these protein components, lipid rafts connect the receptors to their relevant downstream signaling pathways (''focusing'' or ''switching'' effect); hence they also serve as a docking site for adapter and kinase molecules (Simons and Toomre 2000). Based on these observations, the lipid rafts, since they organize receptor clusters of the above molecules, may be regarded as functional units of signaling, the outcome of which is determined by the type and surface density of the protein components.

Besides the composition of lipid rafts, however, there is another important physiological factor tuning the transmembrane signaling: the membrane potential (Tsong and Astumian 1987; Bene et al. 1997). Voltage- and Ca^{2+}-dependent potassium channels are amongst the main candidates responsible for maintaining a potential window necessary for proper signaling in T-lymphocytes (Chandy et al. 1984; Mátyus et al. 1990; Damjanovich and Pieri 1991; Damjanovich et al. 1992a, 1992b; Bacsó et al. 1996; Koo et al. 1997; Jensen et al. 1999). That K^+ channels may be coupled directly or indirectly to the MHC- and IL-2R-containing lipid rafts can be concluded from the following observations: (1) transmembrane signaling via these receptors is accompanied by membrane potential changes [IL-2 cytokine molecules and some antibodies against the MHCII are able to depolarize the cell membrane (Pieri et al. 1992; Bene et al. 1997)]; (2) reversible conformational changes of MHCI molecules induced by de- and re-polarization of the transmembrane electric field have been demonstrated (Bacsó et al. 1996; Bene et al. 1997); (3) the tyrosine and serine kinases involved in MHC and IL-2R signaling pathways modulate the current of K^+ channels (Wade et al. 1993; Bowlby et al. 1997; Chung and Schlichter 1997; Holmes et al. 1997; Martel et al. 1998); (4) disruption of lipid rafts by cholesterol depletion and enriching the membrane with ceramide lead to changes in kinetic and steady-state parameters of K^+ channel currents (Martens et al. 2000; Bock et al. 2003; Hajdú et al. 2003). Irrespective of the nature of the receptor–channel interaction, i.e. whether it is mediated by membrane potential changes or by intracellular messengers, the relative localization of channels and raft components may be an important issue influencing the effectiveness of the receptor–channel coupling (Haugh and Lauffenburger 1997; Kholodenko et al. 2000; Haugh 2002; O'Connel et al. 2004).

By a combination of immunogold labeling and the patch-clamp technique, we studied the relative localization of $K_v1.3$ channels and the MHC-containing lipid rafts in Kit-225-K6 leukemic T-cells. After labeling various receptors of the T-cells with gold nanobeads, the kinetics of binding of *Pandinus imperator* scorpion toxin Pi_2 to the $K_v1.3$ channels were determined. By correlating the patch-clamp data with the morphological parameters of the receptor clusters (sizes and densities) determined by flow cytometric energy transfer (FCET), transmission electron microscopy (TEM), and confocal laser scanning microscopy (CLSM) measurements, we were able to estimate relative proximity of the $K_v1.3$ channels and the investigated receptors.

To demonstrate that our detecting principle works also under other conditions, we show that nanoparticles bound to the MHCI glycoprotein are able to delay binding of an monoclonal antibody (mAb) to the MHCII molecule located in a nanometer-scale vicinity of the MHCI.

Materials and methods

Cell line

The Kit-225-K6 cell line is a human T-cell with helper phenotype and with an IL-2 requirement for its growth (Hori et al. 1987). Cells were cultured in RPMI-1640 medium supplemented with 10% fetal calf serum (FCS), penicillin, and streptomycin (Vereb et al. 2000). Recombinant interleukin-2 (IL-2) (20 U/mL) was also added in every 48 h. The sensitivity of potassium channel currents to specific blockers (Pi_2, TEA) implies that they are of the $K_v1.3$ type in this cell line.

Electrophysiology

Whole-cell measurements were carried out using Axopatch-200 and Axopatch-200A amplifiers connected to personal computers using Digidata 1200 computer interfaces. Standard whole-cell patch-clamp techniques and the pClamp8 software package (Axon Instruments, Foster City, Calif., USA) were used for data acquisition and analysis (Péter et al. 2000). Series resistance compensation up to 85% was used to minimize voltage

xerrors and achieve good voltage-clamp conditions ($V_{err} < 5$ mV). Pipettes were pulled from GC 150 F-15 borosilicate glass capillaries (Clark Biomedical Instruments, UK) in five stages and fire polished, resulting in electrodes having 2–3 MΩ resistance in the bath. The bath solution was (in mM): 145 NaCl, 5 KCl, 1 $MgCl_2$, 2.5 $CaCl_2$, 5.5 glucose, 10 HEPES (pH 7.35). The measured osmolarity of the external solutions was between 302 and 308 mOsm. The pipette solution was (in mM): 140 KF, 11 K_2EGTA, 1 $CaCl_2$, 2 $MgCl_2$, and 10 HEPES (pH 7.2, 295 mOsm).

Physical parameters and application of Pi_2 toxin

The detailed description of the production and purification of *Pandinus imperator* scorpion toxin Pi_2 can be found in Péter et al. (2000). Toxin Pi_2 is a peptide of 38 amino acid length bearing seven positive charges, with a molecular weight of $M_w \approx 4370$ Dalton, an estimated radius of $r \approx 1.11$ nm, and a diffusion constant of $D \approx 2 \times 10^{-6}$ cm^2 s^{-1}. The kinetic constants describing the binding reaction of Pi_2 to the $K_v1.3$ channel in the bath solution have been recently determined: $k_{on} = 2.18 \times 10^8$ M^{-1} s^{-1}, $k_{off} = 6.33 \times 10^{-3}$ s^{-1}, $K_d = 29$ pM (Péter et al. 2000).

Solutions were supplemented with 0.1 mg/mL bovine serum albumin (BSA) to suppress non-specific binding of the toxins to the walls of the tubes and to the Petri dish. Bath perfusion around the measured cell with different test solutions was achieved using a gravity-flow perfusion setup with eight input lines and a PE10 polyethylene tube output tip with flanged aperture to reduce the turbulence of the flow. The solutions were applied in an alternating sequence of control and test solutions, unless stated otherwise. Excess fluid was removed continuously.

Analysis of patch-clamp data

Prior to analysis, whole-cell current traces were corrected for ohmic leak and digitally filtered (using three-point boxcar smoothing). Nonlinear least-squares fits were done using the Levenberg-Marquardt algorithm. Fits were evaluated visually, as well as by the residuals and the sum of squared differences between the measured and calculated data points.

The of wash-in (τ_{in}) and wash-out (τ_{out}) time constants for binding of Pi_2 to the channel were determined by fitting the formulas $I(t) - I_{min} = I_0 \exp(-t/\tau_{in})$ in the wash-in phase and $I(t) - I_{min} = (I_{max} - I_{min})[1 - \exp(-t/\tau_{out})]$ in the wash-out phase to the peak currents plotted versus the time elapsed from switching to bath solution containing the toxin or bath solution only, respectively. Here $I(t)$ is the peak current at time t after addition or removal of toxin, I_0 is the peak current before addition of toxin, I_{min} is the unblocked peak current, and I_{max} is the recovered peak current after wash-out of toxin (Goldstein and Miller 1993).

Monoclonal antibodies and preparation of Fab fragments

The production and specificity of monoclonal antibodies (mAbs) applied in the experimental procedures have been described earlier (Szöllősi et al. 1996). Briefly, mAb MEM-75 (IgG_1) specific to transferrin receptor (TrfR) was kindly provided by Dr. Václav Hořejší (Institute of Molecular Genetics, Academy of Sciences, Prague, Czech Republic). W6/32 (IgG_{2aK}) and L368 (IgG_{1K}) were mAbs developed against the heavy chain of MHCI binding to a monomorphic epitope on the α_2, α_3 domains and the β_2-microglobulin of the MHCI light chain, respectively (Barnstable et al. 1978; Tanabe et al. 1992), and mAb L243 (against MHCII, DR, isotype IgG_{2aK}) (Lampson and Levy 1980) were kindly provided by Dr. Frances Brodsky (UCSF, Calif., USA). mAb anti-Tac (IgG_{2a}) against IL-2Rα was from Thomas A. Waldmann (NIH, Bethesda, Md., USA). The mouse mAb TS2-7.11 (IgG_1) against the very late activation antigen-4 (VLA-4, an $\alpha_4\beta_1$ integrin, CD49a) was purchased from Pierce Biotechnology (Rockford, UK). mAb CD45.2 (IgG_1) against the CD45 receptor was from Prof. S. Meuer (Heidelberg, Germany). These mAbs were prepared from supernatants of hybridomas and were purified by affinity chromatography on protein A-Sepharose. Fab fragments (Fab) of the purified antibodies were prepared by papain digestion at an antibody/enzyme (w/w) ratio of 100, at 37 °C for 4–12 h; for details, see Edidin and Wei (1982) and Matkó and Edidin (1997).

Fluorescent labeling of Fab fragments

Aliquots of the proteins for donor fluorescence were labeled with 6-(fluorescein-5-carboxamido)hexanoic acid, succinimidyl ester (xFITC), and for acceptor fluorescence with 6-(tetramethylrhodamine-5-(and-6)-carboxamido)hexanoic acid, succinimidyl ester (xTRITC), obtained from Molecular Probes (Eugene, Ore., USA). The detailed labeling procedure was described earlier (De Petris 1978; Spack et al. 1986; Szöllősi et al. 1989). Dye-to-protein labeling ratios, which were separately determined for each labeled aliquot in a spectrophotometer, varied between 0.8 and 1.5 (Szöllősi et al. 1989). Fluorescently labeled antibodies retained their biological activity according to competition with unlabeled proteins in binding to membranes of living cells.

Sequential labeling of cells with monoclonal antibodies and immunogold for the patch-clamp experiments

Labeling with the immunogold was carried out according to Jenei et al. (1997) and Vereb et al. (2000). In the first labeling step, freshly harvested cells were washed twice in ice-cold PBS (pH 7.4). The cell pellets were suspended in 100 μL of PBS (1×10^6 cells/mL) and labeled by incubation with approximately 10 μg of

unlabeled whole mAbs (serving as targets for the immunogold beads of anti-Fc fragment specificity in a second step of labeling) for 40 min on ice. To avoid possible aggregation of the mAbs, they were air-fuged (at 9×10^4 rpm, for 30 min) before labeling. The four labeled cells were washed with excess cold PBS twice. Labeling with the unstained whole mAbs was followed by, as a second labeling step, incubation with polyclonal secondary antibodies conjugated to gold beads of 15, 30, or 40 nm diameter (Aurogamig series against the Fc fragment of the unstained whole mAb; from Amersham Pharmacia) or in control experiments with rabbit anti-mouse IgG (RAMIG, from Amersham Pharmacia) on ice for 40 or 80 min.

Wash-in time measurements of the L243 mAb with the patch-clamp

When a stable whole-cell configuration was formed, depolarizing pulses were added to the cell at least five times. The pulses started from a holding potential of −120 mV and rose up to +50 mV for a time interval of 20 ms. The pulses were repeated every 15 s. After the formation of an equilibrium of the current level, 30 μL of L243 mAb solution (2.5 mg/mL in PBS) was pipetted directly onto the cell. The peak current level was continuously monitored by depolarizing pulses, and a gradual decrease was detected, which reached a lower equilibrium in 3–6 min.

Labeling of cells for flow cytometry

Freshly harvested cells were washed twice in ice-cold PBS (pH 7.4), the cell pellet was suspended in 100 μL of PBS (10^6 cells/mL), and labeled by incubation with ~10 μg of xFITC- and xTRITC-conjugated Fabs for 40 min on ice in the dark. The excess of Fabs was at least 30-fold above the K_d during incubation. To avoid possible aggregation of the Fab fragments, they were air-fuged (at 110,000×*g*, for 30 min) before labeling. Special care was taken to keep the cells at ice-cold temperature before fluorescence resonance energy transfer (FRET) measurements in order to avoid unwanted induced aggregations of cell-surface receptors or receptor internalization. Labeled cells were washed with ice-cold PBS and then fixed with 1% formaldehyde. Data obtained with fixed cells did not differ significantly from those of unfixed, viable cells.

Flow cytometric energy transfer

Energy transfer from the excited donor dye to the acceptor labeled receptor population was determined on a cell-by-cell basis in a modified Becton-Dickinson FRCStar^{Plus} flow cytometer equipped with dual laser excitation. The FRET efficiency between the xFITC- and xTRITC-conjugated Fab fragments bound to the cell surface was calculated with specialized software. Detailed methodical descriptions can be found in several earlier publications (Trón et al. 1984, 1994; Szöllősi et al. 1989; Matkó and Edidin 1997; Damjanovich et al. 1998, 1999). The FRET efficiency was calculated by taking into account both the sensitized emission of the acceptor and the quenching of the donor after the necessary correction for the spectral spillovers. The FRET efficiency has an inverse-sixth-power dependence on the donor–acceptor separation; thus the energy transfer has an extremely high sensitivity to changes in distance between donor–acceptor pairs in the range of 2–10 nm (Mátyus 1992). If the donor–acceptor separation distance is larger than the 10 nm effective Förster distance, the energy transfer efficiency falls rapidly to zero; thus we do not attribute significant proximity to the FRET efficiency below 5%.

Determination of the surface expression level of receptors

Constructing energy transfer pairs having sufficiently large acceptor–donor ratios, and the interpretation of our patch-clamp and energy transfer data, made necessary the determination of the cell-surface level of the investigated receptors. The number of binding sites on the cell surface was determined from the mean values of flow-cytometric fluorescence intensity histograms of cells labeled to saturation with xFITC-conjugated Fab fragments (Scatchard analysis). The mean fluorescence intensities were converted into the number of binding sites by calibration with fluorescent microbeads having a known number of fluorescent dyes (Quantum-25 Flow Cytometry Standards, San Juan, Puerto Rico). The diameter of Kit-225-K6 cells was estimated to be 13–14 μm by calibration of the flow-cytometric forward angle light scattering (FALS) signals with beads of known size.

Theory of delayed toxin binding

Direct detection of channels on the cell surface is largely hampered by the exceptionally low level of channels (500–1000 channels per Kit-225-K6 cell, as approximated from the peak currents and the 2–4 pA/channel ratio). Fluorescent monoclonals or specific blockers (e.g. toxins), although available, can only be used with the non-conventional and yet not widely applied single dye fluorescence detection methods requiring highly specialized equipment and technical expertise (Schütz et al. 2000a, 2000b). Furthermore, most of the available monoclonal mAbs bind to the intracellular portion of the channels, making possible only the detection with TEM under non-physiological conditions. Additionally, the specific signals of fluorescent toxins are generally

blurred by the large background due to the unspecific toxin binding.

Therefore, we have sought after an alternative technique for detecting signals specific to the channels, and for revealing possible correlations between the locations of channels and receptors. In our approach we combine the specific immunogold labeling of cell-surface receptors with the high sensitivity of the patch-clamp technique. Our main assumptions are the following: (1) toxin binding to channels can be modulated by gold nanobeads attached to receptors in close proximity (Fig. 1A); (2) the modulation can be detected by monitoring the relaxation times of toxin binding kinetics (wash-in and wash-out times) following concentration jumps of toxin (Bernasconi 1976; Hille 1992; Goldstein and Miller 1993; Péter et al. 2000).

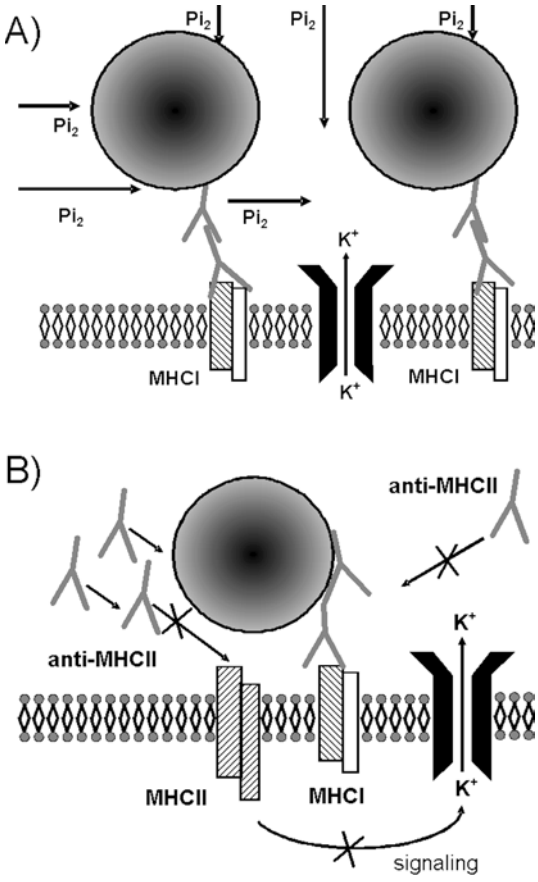

Fig. 1 **A** Schematic drawing illustrating the principle of determination of proximity between ion channels and cell-surface receptors by the patch-clamp technique. Gold nanoparticles of 30 nm diameter bound to the cell-surface receptors, here MHCI, may influence the binding properties of Pi_2 toxin. The modulation of toxin binding properties depend on the size of ligand and nanoparticle, intermolecular distance, and receptor density, as well as the receptor–channel proximity. Because of the 2D nature of the receptor clusters, the lateral component of toxin transport is more severely hindered than the perpendicular one (length of an Fab or Fc fragment is ~6.5 nm; the length of the portion of MHCI or MHCII protruding from the membrane plane is ~10 nm). **B** Illustration of the principle of detection of proximity between two cell-surface receptors (here MHCI and MHCII), one of which (MHCII) when liganded is capable of modulating channel current via some signaling mechanism by retarding ligand (L243 mAb) binding to the "electrically active" receptor (MHCII) by a nanoparticle bound to another receptor (MHCI) in close proximity

The feasibility of our approach had been expected to be guaranteed by the large degree of homo-associations of some of the investigated receptors observed earlier with TEM, CLSM, and near-field scanning optical microscopy (NSOM) (Vereb et al. 2000; Nagy et al. 2001), which suggests the possibility for the creation of extended two-dimensional (2D) gold islands having the potential for modifying ligand binding to cell-surface targets, either by directly blocking the toxin binding sites or by modifying the diffusion rate of the toxin. We have chosen *Pandinus imperator* scorpion toxin Pi_2 as a channel blocker due to its well-described binding characteristics, large affinity and specificity for $K_v1.3$ channels (Gáspár et al. 1995; Péter et al. 1998, 2000, 2001), and due to its relatively large size. Additionally, the antibody coating of the applied gold nanobeads implies the possibility for the formation of a 2D mesh-like structure which is effective in hindering ligand transport, the covering mAbs filling more-or-less the interparticle spaces in the gold islands (Jürgens et al. 1999). Quantitatively, the toxin–channel binding reaction can be treated as one having a 1:1 stoichiometry, described by the k_{on} (M^{-1} s^{-1}) second-order association rate constant and the k_{off} (s^{-1}) first-order dissociation rate constant in the following way (Goldstein and Miller 1993):

$$\text{Channel} + \text{Toxin} \rightleftharpoons \text{Channel:Toxin} \tag{1}$$

According to this scheme, the time constant for relaxation to equilibrium blockade, τ_{in} (wash-in time constant), in the absence of gold labels is described by:

$$1/\tau_{in} = k_{off} + k_{on}c \tag{2}$$

where c designates the toxin concentration. In the presence of gold labels, the effect of the gold can be taken into account by the introduction of an η (≤ 1) factor (which can be termed as "access probability" or "shielding efficiency") in the following way:

$$1/\tau'_{in} = k_{off} + k_{on}\eta c \tag{3}$$

where τ'_{in} designates the increased relaxation time. We assume that the time constant for relaxation to unblocked current levels following toxin removal (or washout time constant), τ_{out}, is not significantly affected by the gold labeling (which is justified by our experiments), i.e. the following relationship is valid:

$$1/\tau'_{out} \approx 1/\tau_{out} = k_{off} \tag{4}$$

Concerning the fraction of unblocked (or remaining) current at equilibrium in the absence of gold, it is related to the rate constants in the following way:

$$f_u = k_{off}/(k_{off} + k_{on}c) \tag{5}$$

with a similar equation when gold is present, by using the η factor:

$$f'_u = k_{off}/(k_{off} + k_{on}\eta c) \quad (6)$$

Dividing Eq. (2) by Eq. (3) and Eq. (6) by Eq. (5), we can see that the wash-in time enhancement (τ'_{in}/τ_{in}) just corresponds to the enhancement of the unblocked current fraction (f'_u/f_u):

$$\tau'_{in}/\tau_{in} = f'_u/f_u = (K_d + c)/(K_d + \eta c) \quad (7)$$

Here we applied the definition of K_d of the toxin:

$$K_d = k_{off}/k_{on} \quad (8)$$

Using Eq. (7), both the wash-in time enhancement and the unblocked current fraction can be used for the determination of the η value, representing the degree of proximity of channels and gold islands, if the K_d of toxin binding and the c toxin concentration are known. However, if we examine Eq. (7) we can recognize that the accuracy of the determination of the η value is larger at larger c concentrations. At concentrations $c >> K_d$, we obtain from Eq. (7) as the limiting case:

$$\tau'_{in}/\tau_{in} \approx 1/\eta \quad (9)$$

which is the largest possible value of τ'_{in}/τ_{in} at a fixed value of η. In our experiments, 2.5 nM ($86\times K_d$) for c was used, implying the validity Eq. (9). Because at high concentrations the remaining (unblocked) current determination can be done with a large error, in these cases the determination of the τ'_{in}/τ_{in} ratio is preferred to f'_u/f_u. Alternatively, the "apparent" association rate constant $k'_{on} = \eta k_{on}$ and the unperturbed rate constant k_{on} can be expressed from Eqs. (2) and (3), and by taking into account Eq. (4) the relative change in k_{on} can be formed:

$$\Delta k_{on}/k_{on} = \eta - 1 \quad (10)$$

The measured τ_{in} values are listed in Table 1, the energy transfer efficiency values are given in Table 2, and the deduced relative changes in k_{on} are listed in Table 3, respectively. A more detailed phenomenological interpretation of the η shielding efficiency in terms of toxin transport and the density of the receptor clusters is given in the Appendix.

Results

Wash-in time constant of Pi_2 toxin binding is differently increased by gold labeling

In the kinetic measurements of toxin binding, four types of samples were studied: (1) unlabeled, control cells; (2) cells incubated with only immunogold to reveal possible effects of nanoparticles (unspecific binding); (3) cells labeled with only the primary antibody against the receptor to reveal possible shielding effects of the antibody layer itself; and finally (4) cells simultaneously labeled with primary antibody and immunogold or with a polyclonal secondary antibody RAMIG as a control to exclude possible effects of the secondary mAbs covering the gold. The measured relaxation times τ_{in} and τ_{out} following jumps of toxin concentration and the deduced binding rates ("apparent" on-rate, k_{on}, and off-rate, k_{off}) are listed in Table 1. Inspecting Fig. 2B–D, significant changes in wash-in time constants can only be seen for some of the "sandwich" samples, i.e. in those cases when the cells were labeled with each of the W6/32, L243, and anti-Tac mAbs and immunogold (52%, 39%, and 26% increments, respectively; t-test values $P < 1\%$). Labeling only with primary mAbs caused only slight, statistically not significant ($< 10\%$), increases in wash-in time constants in all cases. Wash-out times τ_{out} also show no significant differences; the largest difference of ~21% ($P < 25\%$) was observed in the case of immunogold bound to the anti-Tac mAb (Fig. 2D). Wash-in time increment in the presence of gold suggests that gold labeling may exert either a very short-range effect by directly modifying the value of k_{on}, or as a larger range effect it may cause a local depletion of the effective surface concentration of toxin. Because these effects cannot be distinguished in these experiments, and nor can their relative magnitude be determined, we combined all the possible effects of gold in the value of k_{on}, termed by us the "apparent" rate constant. Marked reductions, 40% and 23%, in k_{on} were calculated for the MHC molecules and the IL-2Rα subunit, respectively. While a modest (~14%) reduction was observed for the VLA-4 integrin, no effect was observed in the case of TrfR and CD45 (~2%) (Table 3).

To exclude the possibility for the gold nanobeads to crosslink cell-surface receptors and to induce or alter the degree of the higher order (sub-micrometer scale) clustering, cell samples were incubated with RAMIG as a secondary mAb for 40 or 80 min in the second labeling step. The relaxation times were not affected (t-test value $P < 20\%$), indicating that gold labeling does not change the morphology of the receptor clusters and the observed effects are caused by the large volumes of the gold beads (Table 1, part C). Concerning aspecific binding of the gold nanobeads, we carried out experiments with the gold beads when the primary mAbs were omitted. Changes in relaxation times due to non-specific binding of gold were also negligible (t-test value $P < 30\%$) (Table 1, part C; Fig. 2A).

To compare the hindering effect of nanobeads of different size, the relative changes in k_{on} obtained with gold beads bound to the L243 mAb are listed in Table 5. Although the values show some correlation with the gold size, no significant difference was observed between them ($P < 20\%$).

Regarding the I_0 starting current (measured before addition of toxin), the I_{min} unblocked or remaining current, and the I_{max} recovery current, no significant changes were induced by the immunogold. However, when I_0 values are examined upon binding of antibodies, we notice that the current values are substantially downregulated in the presence of the L243 anti-MHCII mAb (by $\sim 53 \pm 15\%$; Figs. 3 and 5) and the anti-Tac anti-IL-2Rα mAb (by $\sim 48 \pm 24\%$, not shown).

Table 1 Gold-30 nanoparticle-induced hindrance of binding of Pi_2toxins to K_v1.3 potassium channels on the surface of Kit-225-K6 T cells. Measured wash-in and wash-out time constants, and deduced kinetic rates

mAb	Epitope	Unlabeled (control) cells				mAb-labeled cells				mAb and gold-30 labeled cells			
		τ_{in}[b] (s)	τ_{out}[b] (s)	k_{on}[c] (10^{-3} nM^{-1} s^{-1})	k_{off}[c] (10^{-3} s^{-1})	τ_{in} (s)	τ_{out} (s)	k_{on} (10^{-3} nM^{-1} s^{-1})	k_{off} (10^{-3} s^{-1})	τ_{in} (s)	τ_{out} (s)	k_{on} (10^{-3} nM^{-1} s^{-1})	k_{off} (10^{-3} s^{-1})
(A) Raft receptors													
W6/32	MHCI, α_2					30.1 ± 1.4	133.3 ± 21.3	10.3 ± 0.8 L243	7.5 ± 1.2	45.9 ± 4.7	142.9 ± 8.2	5.9 ± 0.9	7.0 ± 0.4
L243	MHCII, DRα	27.3 ± 1.7[a]	119.0 ± 15.6	11.3 ± 1.0	8.4 ± 1.1	28.7 ± 1.6	135.1 ± 21.9	11.0 ± 0.9	7.4 ± 1.2	40.0 ± 3.1	117.6 ± 22.1	6.6 ± 1.0	8.5 ± 1.6
anti-Tac	IL-2Rα					29.9 ± 0.6	135.1 ± 21.9	10.4 ± 0.6	7.4 ± 1.2	37.6 ± 1.6	163.9 ± 26.9	8.2 ± 0.6	6.1 ± 1.0
TS2-7.11	VLA-4					28.1 ± 1.4	136.9 ± 18.8	11.3 ± 0.8	7.3 ± 1.0	30.5 ± 1.3	117.6 ± 5.5	9.7 ± 0.6	8.5 ± 0.4
(B) Non-raft receptors													
MEM-75	TrfR					28.2 ± 0.8	125.0 ± 12.5	11.0 ± 0.5	8.0 ± 0.8	28.1 ± 1.0	121.9 ± 10.4	10.9 ± 0.6	8.2 ± 0.7
CD45.2	CD45	27.3 ± 1.7	119.0 ± 15.6	11.3 ± 1.0	8.4 ± 1.1[a]	29.9 ± 0.8	117.6 ± 9.7	10.0 ± 0.5	8.5 ± 0.7	30.9 ± 1.2	128.2 ± 4.9	9.8 ± 0.5	7.8 ± 0.3
(C) Controls													
Gold-30[d]	–					–	–	–	–	26.1 ± 1.7	131.6 ± 19.0	12.3 ± 1.1	7.6 ± 1.1
RAMIG[e] and L243	MHCII, DRα	27.3 ± 1.7[a]	119.0 ± 15.6	11.3 ± 1.0	8.4 ± 1.1	29.1 ± 2.0	119.5 ± 9.7	9.8 ± 1.3	7.7 ± 0.9	–	–	–	–

[a]The data represent averages and their standard error of mean (SEM) values for five independent measurements, except for the mAb- or gold-labeled IL-2Rα, TrfR, VLA-4, and CD45 receptors, when the number of measurements were seven or eight.

[b]Wash-in and wash-out time constants, τ_{in} and τ_{out}, were determined by fitting the kinetic curves, some examples of which are shown in Fig. 2

[c]The kinetic rate constants k_{on} and k_{off} were determined by using theτ_{in} and τ_{out} time constants as follows:$k_{on} = (1/\tau_{in} - 1/\tau_{out})/c_{tox}$, where c_{tox} is the toxin concentration (2.5 nM); $k_{off} = 1/\tau_{out}$

[d]In this case, only 30-nm gold was added to the cells, without primary antibody. The *t*-test *P* value for the observed change in k_{on}: $P < 30\%$

[e]RAMIG: rabbit anti-mouse IgG, a secondary antibody which binds to the primary L243 mAb on the MHCII. With these samples the incubation times were 40 or 80 min during the second labeling step. The data for the 80-min incubation are indicated. The *t* test *P* value for the observed change in k_{on}: $P < 20\%$

Table 2 Energy transfer efficiency values measured between MHCI, MHCII, VLA-4 integrin, transferrin receptor, and the receptor-type tyrosine phosphatase CD45

	Donor (xFITC-labeled)		Acceptor (xTRITC-labeled)		$E \pm$SEM (%)
	mAb	Antigen	mAb	Antigen	
(A)	L368	MHCI β_2-microglobulin			30.9 ± 3.8[a]
	W6/32	MHCI heavy chain	W6/32	MHCI, heavy chain	20.4 ± 1.8
(B)	L243	MHCII, DRα	W6/32	MHCI, heavy chain	20.6 ± 1.5
	L243	MHCII, DRα			12.3 ± 1.6
(C)	anti-Tac	IL-2Rα	W6/32	MHCI, heavy chain	14.8 ± 0.6
	anti-Tac	IL-2Rα	anti-Tac	IL-2Rα	7.3 ± 0.8
(D)	TS2-7.11	VLA-4, $\alpha_4\beta_1$ integrin	L368	MHCI, β_2-microglobulin	13.7 ± 3.6
			W6/32	MHCI, heavy chain	15.9 ± 1.0
			L243	MHCII, DR α	17.6 ± 2.5
			TS2-7.11	VLA-4, $\alpha_4\beta_1$ integrin	10.6 ± 1.0
(E)	TS2-7.11	VLA-4, $\alpha_4\beta_1$ integrin	MEM-75	TrfR	4.7 ± 2.2
	MEM-75	TrfR	L368	MHCI, β_2-microglobulin	3.5 ± 2.0
	MEM-75	TrfR	MEM-75	TrfR	14.3 ± 1.0
(F)	CD45.2	CD45	L368	MHCI, β_2-microglobulin	2.2 ± 2.0
			W6/32	MHCI, heavy chain	4.0 ± 1.8
			CD45.2	CD45	12.1 ± 3.0

[a]The values represent averages of five independent measurements of transfer efficiency (E) together with their standard error of mean (SEM)

FCET measurements report on nanometer-scale associations

In the hindrance of toxin binding by the gold particles, as well as the characteristics of the gold conjugate, the morphology (size and density) of the nanoparticle-carrying receptor clusters is expected to play an important role. We have therefore conducted FRET measurements aimed at the determination of the degree of homo- and hetero-clustering of the receptors used in the patch-clamp experiments. Based on the FRET efficiencies and the expression levels of receptors, inter-receptor separations, the number of bound gold particles, and the average number of clusters for the different receptors could be estimated and correlated with the measured changes in toxin association rate (Table 3).

FRET efficiency measured between donor- and acceptor-labeled mAbs bound to the same type of receptor indicate the degree of homo-association. Inspecting the data in Table 2, the strongest homo-association is shown by the MHCI antigen (20% FRET); medium ones by the MHCII glycoprotein, VLA-4 integrin, and CD45 phosphatase (11–12%); and the weakest one by the IL-2Rα subunit (7%) (Fig. 4A, B). The largest 31% FRET efficiency measured between the β_2-microglobulin and heavy-chain subunits of the MHCI is mainly of intramolecular origin and serves as a positive control for the FRET measurements (Fig. 4A). The different degree of hetero-association of the receptors indicates their heterogeneity in raft distribution, i.e. their tendency to belong to the same signaling platform. FRET efficiency measured between mAbs bound to receptors of different type reports on the degree of hetero-association. The large ~21% FRET efficiency measured between mAbs on MHCI and MHCII indicates a strong molecular level co-clustering of these receptors (Table 2, part B; Fig. 4B). Although to a somewhat smaller degree, a significant co-clustering is indicated by the ~15% FRET efficiency obtained between IL-2Rα and MHCI (Table 2, part C; Fig. 4C).

The biological role of adhesion receptors in the formation of the immune synapses (places of interaction of MHCI and T-cell receptor on two opposing cell surfaces in contact) suggests that VLA-4 integrins localize in the MHC-containing lipid rafts. The large 14–18% FRET efficiencies measured between VLA-4 and MHCI or MHCII demonstrate a close proximity of the VLA-4 to components of the MHC rafts (Table 2, part D; Fig. 4D).

Concerning raft localization of TrfR and CD45, no FRET (2–4%) was measured between each of these receptors and MHCI (Table 2, parts E, F; Fig. 4C, D). The lack of FRET in these cases implies that TrfR and CD45 receptors locate in cell-surface compartments different from the MHC raft. This is further supported by the lack of FRET observed between the cholera toxin B subunit (specifically labeling the MHC-containing GM_1 lipid rafts) and CD45 or TrfR (data not shown). Additionally, the lack of FRET observed between TrfR and CD45 implies that CD45 is excluded not only from the MHC rafts but also from the coated pits (data not shown).

Immunogold on the MHCI changes the kinetics of binding of L243 mAb to the MHCII

Based on the aforementioned nanometer-level close proximity of the MHCI and MHCII antigens and the observed down-regulation exerted by L243 mAb on the K^+ channel currents, we examined the kinetics of the L243 mAb binding to the MHCII glycoprotein in the

Table 3 Surface expression level, intermolecular separation, and average cluster size for receptors and 30-nm gold nanoparticle induced relative change in k_{on} of Pi_2 toxin binding

mAb	Epitope	Relative change in k_{on}	Significance value of t-test	Receptor expression level	Intermolecular separation by FRET	Number of bound gold-30	Average cluster size by CLSM	Number of clusters
		$\Delta k_{on}/k_{on}$ (%)	$P <$ (%)	B (%)	d (nm)	$N_{gold\text{-}30}$ ($\times 10^3$)	$R_{cluster}$ (nm)	$N_{cluster}$
(A) Raft receptors								
W6/32	MHCI, α_2	$-42.7 \pm 9.8(5)$[a]	1[b]	100.0 ± 13.3[c]	7.0 ± 0.1[d]	38.9 ± 5.2[e]	700 ± 93[f]	31.8 ± 9.5[g]
L243	MHCII, DRα	$-40.0 \pm 10.3(5)$	1	76.6 ± 8.6	7.8 ± 0.2	37.1 ± 4.6	680 ± 136	32.1 ± 13.4
anti-Tac	IL-2Rα	$-21.5 \pm 7.0(8)$	2.5	34.2 ± 8.3	8.6 ± 0.2	20.0 ± 4.9	600 ± 46	22.4 ± 6.4
TS2-7.11	VLA-4	-14.2 ± 8.1 (7)	10	< 4.0	8.1 ± 0.2	< 2.1	–	–
(B) Non-raft receptors								
MEM-75	TrfR	$-1.1 \pm 7.2(8)$	45	15.3 ± 1.5	7.5 ± 0.1	6.8 ± 0.7	200 ± 33	68.5 ± 23.7
CD45.2	CD45	$-2.0 \pm 6.7(8)$	40	28.7 ± 5.0	7.8 ± 0.3	13.9 ± 2.6	–	–

[a]Data represent averages and their standard error of mean (SEM) values for independent measurements, the number of which is indicated in parentheses. These values were calculated by using the kinetic data in Table 1. The k_{on} values measured in the presence of both mAb and gold-30 were compared with those measured in the presence of only the primary mAb. The P values of significance (probability of observing a given value or larger) for a one-sided t-test carried out between relative changes in k_{on} for the same receptor pairs are the following: MHCI–TrfR, $P < 0.5\%$; IL-2Rα–TrfR, $P < 5\%$; VLA-4–TrfR, $P < 15\%$; MHCI–IL-2Rα, $P < 5\%$; VLA-4–IL-2Rα, $P < 30\%$; and MHCI–VLA-4, $P < 2.5\%$

[b]The maximum P values of significance of the t-test were computed based on the means and errors listed in Table 1

[c]Expression levels of receptors were determined by flow cytometric fluorescence intensity measurements of cells labeled by fluorescently tagged antibodies; 100% means $(1.0\text{–}1.5)\times 10^6$ binding sites. The difference in the expression levels for the MHCI–MHCII and the IL-2Rα–CD45 pairs are not significant; t-test values: $P < 10\%$ and 30%, respectively (number of measurements, $n = 5$)

[d]Intermolecular separations were determined from the energy transfer efficiency data listed in Table 3 using the Förster formula, $d = R_0(1/E - 1)$, with $R_0 = 5.6$ nm, a characteristic Förster distance for the xFITC–xTRITC donor–acceptor dye pair (Van Der Meer et al. 1994). Error values for the distance were determined from the corresponding errors in FRET values, by application of the Gaussian propagation law of error on the Förster formula (number of measurements, $n = 5$)

[e]An upper limit for the number of bound gold-30 particles was calculated as $N_{gold\text{-}30} = B(d/a)^2/\pi$, with the absolute copy number of receptor $B = (\%$ expression level$)\times 10^6$, inter-receptor distance d, and the effective radius of the secondary antibody coated gold-30 ≈ 15 nm + 5 nm = 20 nm. In this calculation the receptors are assumed to constitute a single continuous receptor island which is covered by the gold beads at zero distance of closest approach. The real values of the bound gold beads can be smaller due to losses during sample preparation. The differences for the MHC–IL-2Rα pairs are significant ($P < 2.5\%$); those for the MHCI–MHCII and the IL-2Rα–CD45 pairs are not significant ($P < 45\%$ and 20%, respectively)

[f]Average cluster radii of the indicated receptors are taken from Vereb et al. (2000). The radii for the MHC and IL-2Rα molecules are not different significantly, in good accordance with the fact that they belong to the same type of lipid raft

[g]Number of clusters of each indicated size was approximated as $N_{cluster} = B(d/R_{cluster})^2/\pi$, with the absolute copy number of receptor $B_{cluster} = (\%$ expression level$)\times 10^6$, inter-receptor distance d, and the average cluster size $R_{cluster}$. In deducing this formula, the area covered by the receptors is divided by the area of a receptor cluster of radius R. Error values were determined by application of the Gaussian propagation law of error. The t-test values for the MHC–IL-2Rα and MHC–TrfR pairs: $P < 25\%$ and $P < 15\%$, respectively

presence and absence of 30-nm gold bound to the MHCI molecule via the W6/32 mAb (Fig. 1B). This experiment is an extension of that carried out with the Pi_2 toxin; it demonstrates that proximity between an "electrically active" (MHCII) and "silent" (MHCI) receptor can be monitored on the nanometer scale by the patch-clamp technique using our "delayed binding" principle. Wash-in times (τ_{in}) and unblocked current fractions (I_{min}/I_0) in the presence and absence of gold are presented in Table 4. From the data in part B we can learn that gold labeling of MHCI causes a ~2.3-fold wash-in time increase of L243 mAb binding (t-test value $P < 2.5\%$). The concomitant 30% enhancement in unblocked current fraction is not significant statistically ($P < 20\%$). In this case, channel gating might be modulated by intracellular messengers and the effect induced by the L243 mAb cannot be reversed on the time scale of the experiment; consequently the wash-out time constant (τ_{out}) and the association rate constant k_{on} (depending on τ_{out}) cannot be determined.

Figure 5 shows the wash-in phases of the L243 mAb binding kinetics: without gold and W6/32 mAb (Fig. 5A), with W6/32 mAb and without gold (Fig. 5B), and with gold bound to W6/32 mAb (Fig. 5C). According to Table 4 (parts A and B) and Fig. 5B, binding of W6/32 mAb alone can cause only a negligibly small enhancement in the wash-in time constant and unblocked current fraction.

In view of the fact that CD45 phosphatase is located outside of the MHC rafts, as a negative control we attached the gold to the CD45 via the CD45.2 mAb, and examined the degree of modulation of the kinetics of binding of the L243 mAb to the MHCII; no significant changes were observed (Table 4, part C).

Discussion

Correlation between the retardation of toxin binding and the density and raft localization of receptors

The effect of gold nanobeads can be explained by the combined evaluation of the present FRET data and the CLSM, as well as TEM results obtained earlier on

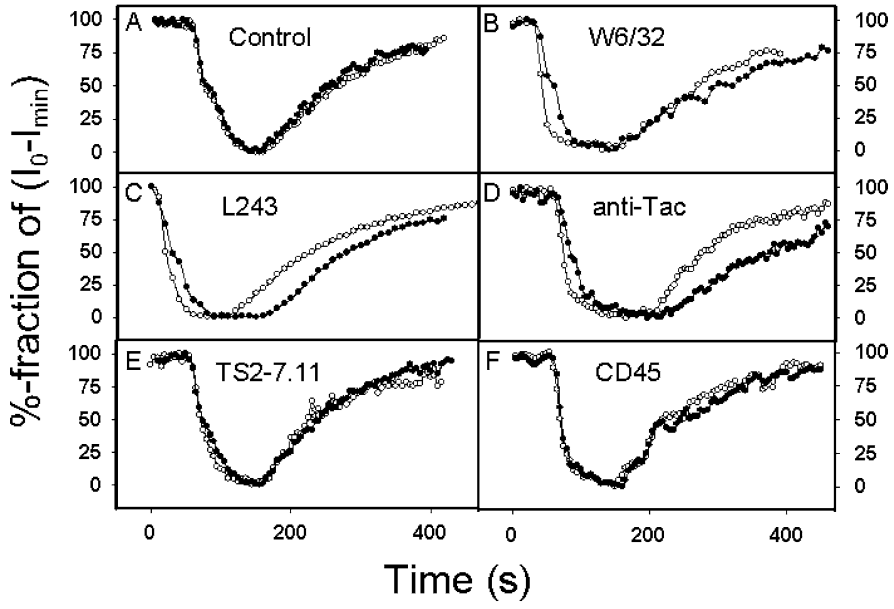

Fig. 2A–F Representative wash-in and wash-out kinetic relaxation curves of binding of Pi_2 toxin to $K_v1.3$ channels in the absence (*empty circles*) and in the presence of immunogold nanoparticles (*solid circles*). **A** Unlabeled control cells. **B–F** Cells labeled by the indicated primary mAbs (W6/32 anti-MHCI heavy chain, L243 anti-MHCII DRα, anti-Tac anti-IL-2Rα, TS2-7.11 anti-VLA-4, CD45.2 anti-CD45) prior to addition of goat-anti-mouse-IgG (GAMIG) conjugated immunogold of 30 nm diameter. Cells in whole cell configuration were depolarized from a holding potential of −120 mV to +50 mV every 15 s. The peak currents $I(t)$ were normalized to the difference in equilibrium levels of peak currents before and after blocking with toxin, I_0 and I_{min}, respectively. These values are plotted as a function of time

Kit-225-K6 cells (Vereb et al. 2000; Nagy et al. 2001). We have summarized in Table 3 the relative changes in k_{on} geometrical parameters of the clusters, such as the inter-receptor distances and average cluster radii, the number of bound gold beads, and the number of clusters. Data in Table 3 suggest that not only the cluster morphology but also the raft localization of the receptors should play a role in the hindering effect.

The largest modulation of −40% was obtained with the two major raft proteins MHCI and MHCII, in a good correlation with the fact that they form the most extended and dense clusters (Table 3, part A). Earlier CLSM and TEM analyses revealed that both MHCI and MHCII form clusters of ∼700 nm average diameter. The TEM images show that smaller scale inhomogeneities, "quasi confluent" gold islets comprised of ∼20 gold beads with inter-particle spacings of just a few nanometers, occur with high frequency (fig. 7 in Vereb et al. 2000 and fig. 6 in Nagy et al. 2001). The small, 7–8 nm inter-receptor distance of the MHC proteins, calculated from the 12–20% FRET efficiency (Table 2, part A), also can give rise to cluster fluctuations of this kind. Clearly, the gaps between the adjacent nanobeads in these gold islets are small enough to effectively hinder the surface diffusion of toxins prior to reaching their destinations. Additionally, in the case of the close proximity (< 10 nm) of gold particles and channels, even direct modulation of k_{on} can also be expected.

A modest, −22%, effect was observed with the IL-2Rα subunit (Table 3, part A). Although IL-2Rα forms clusters similar in size to those of the MHCs, their density is significantly smaller due to the smaller receptor expression level and the larger inter-receptor distance (8.6 nm and 7–7.8 nm for the IL-2Rα and the MHCs, respectively; see also figs. 1, 5, and 7 in Vereb et al. 2000; fig. 6 in Nagy et al. 2001). The fact that, similarly to the MHC case, gold on the IL-2Rα can influence toxin binding is reasonable, because IL-2Rα localizes in the MHC rafts (Table 2, part C).

In view of the close proximity of VLA-4 integrin to $K_v1.3$ channels reported earlier on other cell types and its role in the formation of the immune synapse, we involved this receptor in our investigations (Levite et al. 2000; Levite 2001). Based on the close proximity between the VLA-4 integrin and the MHCs (Table 2, part D), we would expect that gold on VLA-4 may also modify the binding kinetics of the toxin. The insignificant modulation seems to be due to the very low receptor expression level and the small cluster size rather than to a direct steric modulation of k_{on} by the gold on the VLA-4 adjacent to the $K_v1.3$ channel (Table 3, part A). Although a modest FRET was observed between VLA-4 integrins, their very low expression level makes possible the formation of at most dimers, not effective in hindering toxin binding. Although both TrfR and CD45 are homo-associated (7.5–7.8 nm inter-receptor distance), no hindering effect was observed in these cases (Table 3, part B). For the TrfR, the lack of effect can equally be attributed to the very low expression level, to the highly fragmented clustering, and to the fact that it is located in membrane compartments (clathrin-coated pits) different from the MHC rafts (Mátyus et al. 1995). The different localization of TrfR on these cells is justified by the small FRET between TrfR and MHCI or

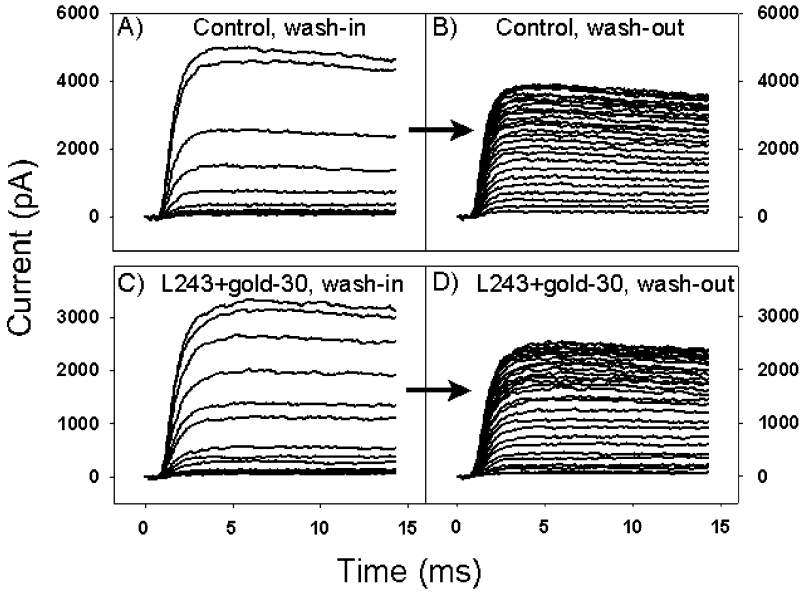

Fig. 3 Representative current–time traces measured during the wash-in and wash-out phases of Pi_2 toxin concentration relaxation experiments on unlabeled control cells (**A**, **B**) and on cells labeled with GAMIG-conjugated immunogold of 30 nm diameter tethered to the MHCII glycoprotein via the L243 primary mAb (**C**, **D**). The large reduction in starting current (ca. 5 nA vs. 3 nA) can be attributed the receptor modulation of the channel by the liganded MHCII receptor (see also Results). Cells in the whole cell configuration were depolarized from a holding potential of −120 mV to +50 mV every 15 s. Perfusion with control extracellular normal Ringer (NR) solution was applied until the current amplitude stabilized. Protocols in **A** and **C**: recording on cells in the absence or presence of gold, the perfusion was switched to NR solution containing 2.5 nM Pi_2 toxin at the end of the first trace shown. Repetitively obtained current traces are presented until the equilibrium block by the toxin was reached. **B** and **D**: on the same cells, being in equilibrium block described in **A** and **C**, perfusion was switched back to control NR solution. All current records were leak-subtracted. Sampling rate was 20 kHz and a 2 kHz low-pass filter was applied

VLA-4 (Table 2, part E), as well as by earlier CLSM and TEM observations (Vereb et al. 2000).

Based on the nearly equal receptor expression levels and the same degree of homo-clustering of CD45 and IL-2Rα, the different effects observed with these receptors can equivocally be attributed to their different raft localizations. This observation shows clearly that our hindered binding approach can be used for monitoring the proximity. Concerning biological function, the different raft localization of CD45, which has been demonstrated by several other groups in both T- and B-cells (Cheng et al. 1999; Janes et al. 1999; Su et al. 2001; Giurisato et al. 2003), can be attributed to the role of this receptor in the negative feedback control of the transmembrane signaling processes triggered by the phospho-kinases. In view of the obtained hindering effects, we postulate for the first time that $K_v1.3$ channels are located in the MHC-containing lipid rafts or close to them, at most at a distance comparable to the effective particle size (30–40 nm, the sum of the gold diameter and the size of the tethering mAb) (Murphy et al. 1988; Jürgens et al. 1999).

The hindering effect weakly depends on the gold size

The insignificant differences obtained between the delaying effects of nanobeads of different size (Table 5) can be explained by a combination of two opposing effects: (1) with increasing size, the number of bound gold beads is smaller due to steric hindrance during binding; (2) the increased size represents an enhanced sphere of action of the nanobeads, i.e. larger obstacles for the toxins. From the weak linear correlation between the observed changes and the gold size, we can conclude that the second effect is the dominating one. The weak increase in the net effect can be explained by the fact that, although increasing the bead size leads to a reduction in density, with the larger gold beads, besides the hindering of 2D diffusion, even hindering of 3D diffusion begins to play a larger role.

$K_v1.3$ is located in the vicinity of the MHC-containing lipid rafts

The lack of modulation of wash-in time in the case of nanobeads attached to CD45 or TrfR as negative controls lends support to the conclusion that wash-in time enhancements of the MHC and IL-2Rα molecules should reflect not only the cluster morphology but also the proximal locations of the $K_v1.3$ channels to the gold islands created on these receptors. We can conclude that $K_v1.3$ channels localize either inside or in the nanometer-scale (30–40 nm) proximity of the MHC rafts. The possibility of molecular scale proximity between the $K_v1.3$ channels and the MHC rafts is further supported by the following observations: (1) the down regulation of $K_v1.3$ current by antibody engagement of the MHCII and IL-2Rα (Bene et al. 1997); (2) modulation of kinetic

parameters of $K_v1.3$ channels induced by changing membrane cholesterol or ceramide level in T-cells (Bock et al. 2003; Hajdú et al. 2003); and (3) co-localization of VLA-4 and $K_v1.3$ channels on T-cells (Levite et al. 2000; Levite 2001).

Although the mechanism behind the depolarizing effect induced by antibody engagement of the MHCII or IL-2Rα is not yet clear, nanometer-scale proximity of potassium channels and these receptors would amplify signaling independently, whether this effect is evoked directly (via steric interaction of the binding mAb and channel) or indirectly (via downstream signaling pathways).

Detection of receptor proximity by delaying receptor modulation of ionic channels

Our principle of probing proximity by the detection of binding kinetics with the patch-clamp technique can be extended to any pair of receptors, one of which is capable of channel regulation. Our major assumption is that binding of a ligand to an "electrically active" receptor can be delayed by binding nanoparticles of sufficient size to another receptor in close proximity. The hindrance in binding of a ligand to the "electrically active" receptor should lead to a measurable change in the time course (rate constants or plateau values of current) of channel regulation. Special hormone–receptor systems, e.g. TSH (Kiss et al. 1997) and IL-2 (Bacsó et al. 1996), and some antibody–antigen systems capable of modifying the membrane potential, are amongst the possible candidates for this kind of experiment. Studying the co-localization of receptors with the high-sensitivity patch-clamp technique may be especially advantageous when, for example, the "electrically active" receptors are expressed at a very low level, the detection of which is hardly accessible by conventional fluorescence techniques, or when the immunofluorescent labeling techniques cannot be applied for some reason (e.g. lack of mAb). In our channel blocking experiments, we observed significant reduction in the channel current (the mechanism of which is currently under investigation) upon binding of L243 and anti-Tac whole mAbs to the MHCI and IL-2Rα molecules (~53% and ~48% decrease, respectively). Earlier we have reported on depolarization of the membrane potential upon antibody engagement of MHCII on JY B-lymphoblast cells (Bene et al. 1997) and upon IL-2 engagement of the IL-2 receptor on HUT-102B2 T-lymphoblast cells (Pieri et al. 1992). These observations parallel well with the finding that both receptors are elements of the same transmembrane signaling platform, termed by us MHC rafts on these cell lines (Bene et al. 1994, Matkó et al. 2002). In view of the high proximity of MHCI and MHCII, their highly overlapping large-scale molecular clusters (Vereb et al. 2000), and the aforementioned channel regulating capability of MHCII, we applied our detecting principle to the MHCI–MHCII receptor pair. The immunogold bound to the MHCI via the W6/32 mAb significantly enhanced the wash-in time of the L243 mAb during binding to the MHCII and only to a small extent the remaining (unblocked) current fraction. Concerning the reason for the wash-in time enhancement, hindrance of surface diffusion of L243 prior to binding to MHCII and direct shielding of the L243-binding epitope by the gold can equally play a role.

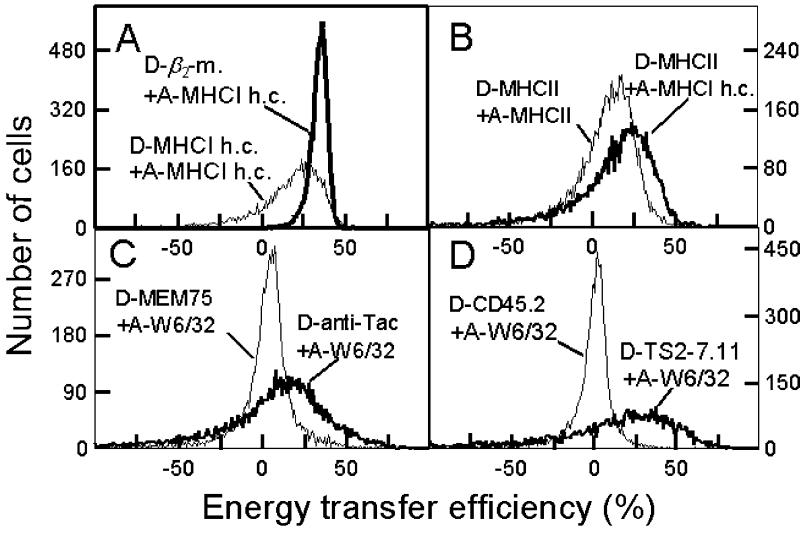

Fig. 4 Flow cytometric energy transfer (FCET) efficiency histograms collected on 10^4 cells. FRET efficiency was measured by the FCET method between donor- and acceptor-conjugated Fab fragments bound to the indicated cell surface receptors on a cell-by-cell basis. Used Fabs: L368, anti-MHCI light chain (β_2-microglobulin); W6/32, anti-MHCI heavy chain; L243, anti-MHCII DRα; anti-Tac, anti-IL2Rα; TS2–7.11, anti-VLA- 4; CD45.2, anti-CD45. Designations: D, donor (xFITC); A, acceptor (xTRITC); β_2-m, β_2-microglobulin; MHCI hc, MHCI heavy chain. The high intramolecular FRET efficiency (30%) measured between the β_2-microglobulin and MHCI heavy chain serves as a positive control for close proximity. Note that the widths of the frequency distributions are inversely proportional to the expression levels of receptors labeled by the donor-conjugated Fabs. The mean values of similar histograms were averaged over the independent measurements and tabulated in Table 2

Table 4 Nanoparticle-assisted hindrance in L243 mAb-induced modulation of $K_v1.3$ potassium channel currents on the surface of Kit-225-K6 T-cells. Measured wash-in time constants and remaining current fractions

Sample	τ_{in}[b] (s)	I_{min}/I_0[b] (%)
(A) Control		
Unlabeled cells	8.3 ± 2.8[a]	34.4 ± 10.1[a]
(B) Raft receptor		
W6/32-labeled	11.3 ± 4.2	35.7 ± 8.1
W6/32- and gold-30-labeled	37.4 ± 9.5	45.8 ± 6.7
(C) Non-raft receptor		
CD45.2-labeled	10.7 ± 3.2	31.1 ± 6.3
CD45.2- and gold-30-labeled	11.9 ± 8.6	35.6 ± 4.9

[a]The data represent averages and their standard error of mean (SEM) values for four independent measurements. The P values of significance of t-test carried out between: (1) τ_{in} values for the W6/32–(W6/32 + gold-30) pair: $P < 2.5\%$; (2) τ_{in} values for the (CD45.2 + gold-30)–(W6/32 + gold-30) pair: $P < 5\%$; and (3) I_{min}/I_0 values for the W6/32–(W6/32 + gold-30) pair: $P < 20\%$

[b]Wash-in time constant and the unblocked current fraction in the presence of L243 mAb, τ_{in} and I_{min}/I_0, respectively, were determined from the respective kinetic curves, some examples of which are shown in Fig. 5

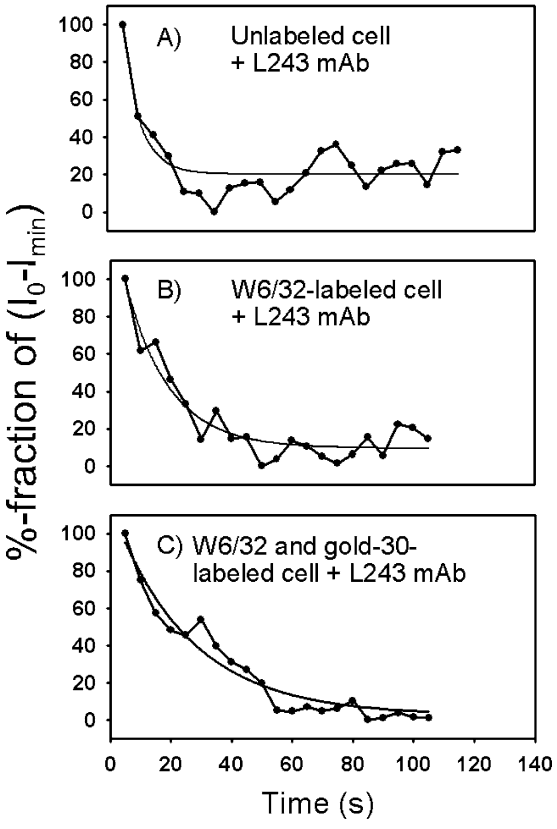

Fig. 5 Representative relaxation curves showing the effect of gold-labeling of MHCI on the indirect blocking of $K_v1.3$ channels induced by L243 mAb engagement of the MHCII glycoprotein. The wash-in time parameter is significantly enhanced in the presence of immunogold. Because, in this case, the channel current is supposed to be blocked by intracellular signaling pathways, this effect is not reversible on the time scale of the measurement (as opposed to the reversible direct blocking effect of Pi_2 toxin). As a consequence, the wash-out phases are missing. The lines labeled by *solid circles* are the experimental curves; those *without label* are fitting exponential curves of the type $I(t) - I_{min} = (I_0 - I_{min})\exp(-t/\tau_{in})$, from which the wash-in time constant t can be determined. The peak currents $I(t)$ were normalized to the difference in equilibrium levels of the peak currents before and after blocking with L243 mAb, I_0 and I_{min}, respectively

Besides demonstrating the feasibility of our principle of detecting proximity by the delaying of ligand binding, this experiment also serves as a positive control for the toxin-binding experiments by presenting a case when the hindering nanoparticle and the binding site for the hindered ligand are located at a well-determined small distance from each other. By taking into account that Pi_2 toxin and L243 mAb have similar sizes, diffusion and binding properties [$r_{Pi2} = 1.11$ nm, $D_{Pi2} = 1 \times 10^{-6}$ cm^2 s^{-1} (Tokita et al. 1996), $K_{d,Pi2} = 29$ pM, $k_{on,Pi2} = 4.6 \times 10^{-13}$ cm^2 s^{-1} (Péter et al. 2001); $r_{L243} = 3.6$ nm, $D_{L243} = 0.7 \times 10^{-6}$ cm^2 s^{-1}, $K_{d,L243} = 1$ nm, $k_{on,L243} = 0.5 \times 10^{-13}$ cm^2 s^{-1}], we expect the hindering principle to operate also when gold and potassium channels are in nanometer-scale proximity. This expectation is further supported by the fact that association reactions of both ligands are similarly reaction limited, which is indicated by their small Damköhler numbers ($D_a << 0.1$). The D_a Damköhler number, which indicates the relative contribution of chemical binding and diffusion in the association reaction, is defined by $D_a = k_{on}/(4\pi D a_{cell})$, where k_{on} is the association rate constant, D is the 3D diffusion constant, and $a_{cell} \approx 7$ μm is the cell radius (Haugh and Lauffenburger 1997). Although the mechanism of cur-

Table 5 Gold size dependence of the hindering effect

mAb	Epitope	Type of immunogold	Effective diameter (nm)	Relative change in k_{on}, $\Delta k_{on}/k_{on}$ (%)	Number of bound gold beads, N_{gold} ($\times 10^3$)
L243	MHCII, DRα	Gold-15	25[a]	-35.7 ± 10.2	94.9 ± 11.7
		Gold-30	40	-40.0 ± 10.3	37.1 ± 4.6
		Gold-40	50	-54.5 ± 11.6	23.7 ± 2.9

[a]The width of the coating secondary antibody layer (~5 nm) should be added to the radius of the gold beads

[b]Data represent averages and their standard error of mean (SEM) values for five independent measurements. These values were calculated similarly to those in Table 3. The k_{on} values measured in the presence of both L243 mAb and gold were compared with that measured in the presence of only the L243 mAb. The P values of significance in the t-test carried out between relative changes in k_{on}: (1) for the (gold-40)–(gold-30) pair: $P < 20\%$; (2) for the (gold-40)–(gold-15) pair: $P < 15\%$

[c]Upper limit for the number of bound gold particles was computed according to footnote e of Table 3

rent modulation by the anti-Tac and L243 mAbs is under investigation, the fact that antibody engagement of IL-2Rα and MHCII changes the channel current in the same direction well parallels the observation that both receptors are components of the same signaling unit, i.e. of the same MHC raft (Fig. 6). The insensitivity of the I_{min} unblocked current to the changing "apparent" k_{on} (Eq. 7) can be attributed to the large applied toxin concentration. Because changes in wash-in time are larger for large toxin concentrations (see "Theory of delayed toxin binding", above), these experiments were carried out at a toxin concentration much larger than K_d (2.5 nM vs. 29 pM).

Biological role of the co-localization of $K_v1.3$ with the MHC rafts

In view of (1) the well-established role of the IL-2 receptor complex in T-cell activation (Nelson and Willerford 1998), (2) the active role of VLA-4 integrins in the formation of immune synapse and in cell locomotion (Levite et al. 2000; Levite 2001; Bacsó et al. 2002), and (3) the active roles of the MHC glycoproteins in the initiation of transmembrane signaling cascades leading to, for example, apoptosis (Wade et al. 1993; Skov et al. 1997, 1998; Altomonte et al. 1999; Drénou et al. 1999; Huby et al. 1999), the localization of $K_v1.3$ channels in the vicinity of the MHC rafts may play a role in speeding up membrane potential-mediated signaling effects. The speeding up itself may occur by shortening the time for diffusional translocation of signaling molecules between the sites of the receptors and channels (Haugh and Lauffenburger 1997; Kholodenko et al. 2000; Haugh 2002; O'Connell et al. 2004).

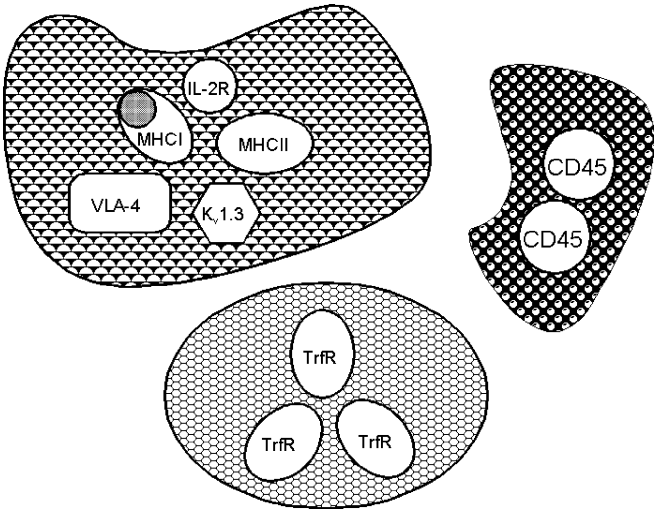

Fig. 6 Membrane compartmentalization of the investigated receptors. MHCI and MHCII glycoproteins, IL-2Rα subunit, and the VLA-4 integrin are all components of the same GM_1 lipid raft. Transferrin receptor (TrfR) and CD45 are located in different compartments. $K_v1.3$ channels localize inside or in the nanometer-scale vicinity of MHC-containing lipid rafts

Conclusions

Reduction of association rate constant of *Pandinus imperator* scorpion toxin Pi_2, an efficient blocker of $K_v1.3$ channels, has been observed in the presence of 30-nm immunogold bound to the cell-surface receptors MHCI, MHCII, IL-2Rα, and VLA-4, all shown to be components of the same lipid raft on Kit-225-K6 T-lymphoma cells. After determination of inter-receptor spacings of the receptors by simultaneously conducted FRET measurements, the effect has been shown to correlate with the density and size of the homo-clusters. From the observation that immunogold bound to the non-raft CD45 or TrfR did not modify the binding rate of the toxin, we conclude that the effect is sensitive not only to the morphology of receptor clusters but also to the relative spatial localizations of $K_v1.3$ channels and cell-surface receptors. The $K_v1.3$ channels have been shown to localize in the nanometer-scale vicinity of the MHC-containing lipid rafts. In a second type of experiment, receptor modulation of the channel current induced by antibody binding is delayed by immunogold nanoparticles bound to another receptor in close proximity. We propose a method for detecting receptor–channel or inter-receptor proximity by a combination of the patch-clamp technique with the delaying of ligand binding by nanoparticle clusters. Co-localization of $K_v1.3$ channels with MHC-containing lipid rafts may speed up the initial phases of membrane potential-mediated signaling events by spatially confining the stimulating receptors and the effector channels.

Acknowledgements This work was financed by grants OTKA T042618 and TS040773 to S.D., grants OTKA T043087 and ETT 222/2003 to R.G., and by grant ETT 138/2001 and a Békésy György postdoctoral fellowship to L.B.

Appendix

Phenomenological interpretation of the η shielding factor

Analogous problems concerning constrained 3D diffusion of particles in a background of retarding obstacles of various sizes and shapes were treated by theorists modeling phenomena in the field of gel electrophoresis and size exclusion chromatography (Schnitzer 1988; Tong and Anderson 1996). In the case of the close proximity of gold islands and channels, the effective local concentration of toxin around the channels can be reduced by two effects: (1) steric exclusion due to the finite size of the gold beads and the covering antibodies (Schnitzer 1988; Minton 1992; Jürgens et al.

1999), and (2) the reduced diffusion rate of toxin in the gold island due to the increased hydrodynamic interaction caused by the volume confinement (Han and Herzfeld 1993; Tomadakis and Sotirchos 1993; Tong and Anderson 1996; Phillips 2000).

The diffusion current of the toxin can be decomposed into two components: one is parallel to the cell surface; the other is perpendicular to it (Fig. 1A). Because the gold islands are mainly laterally extended, i.e. 2D systems, we expect the lateral component of diffusion to be more effectively reduced than the perpendicular one. Moreover, the binding of toxin to the channel is necessarily preceded by a surface diffusion step or reduction-in-dimensionality (RD) enhancement (Berg and Purcell 1977; Wang et al. 1992; Axelrod and Wang 1994), which further emphasizes the significance of the lateral component of the diffusion current. A semi-quantitative interpretation of the η shielding efficiency can be made, based on the work of Axelrod and Wang (1994) discussing the role of RD enhancement for reaction-limited association of ligands with cell-surface receptors. That binding of toxin to the $K_v1.3$ channels is reaction limited is justified by the small value of the Damköhler number ($D_a < 10^{-4}$), calculated by using the values of k_{on} and the diffusion constant of the toxin, as well as the cell radius given in Materials and methods (Haugh and Lauffenburger 1997). Based on the work of Axelrod and Wang (1994), the following formula can be deduced for the RD enhancement factor of the k_{on} association constant:

$$\frac{k_{on}}{k_{on}^{(0)}} = \frac{1 + 16\chi_2 D_2 K_u/(3\pi\chi_3 D_3 a_{cell})}{1 + 16\chi_2 D_2 K_u/[(3\pi\chi_3 D_3 a_{cell}) + 2\sigma k_{off}/(a_{cell} c)]} \quad \text{(A1)}$$

where D_2 and D_3 designate the 2D (on the cell surface) and 3D (off the cell surface) diffusion constants, χ_2 and χ_3 are the 2D and 3D success probabilities per encounter (orientation factor) leading to binding, K_u is the unspecific equilibrium binding constant of toxin onto the membrane, a_{cell} is the cell radius, k_{off} is the dissociation rate constant of the toxin from the channel, σ is the average free path length of the toxin (taken to be equal for 2D and 3D diffusion), c is the toxin concentration, and $k_{on}^{(0)}$ is the association rate constant in the absence of surface diffusion of toxin, i.e. at $D_2 = 0$. Equation (A1) tells us that surface diffusion can be effective whenever unspecific binding to the surface is strong, i.e. K_u is large (as is the case with the Pi_2 toxin, due to its seven positive charges) and when c is small enough. Additionally, Eq. (A1) reports that gold islands may cause a reduction in D_2 and χ_2 much more than in D_3 and χ_3, because of the large lateral 2D nature of gold islands, and as a consequence the value of k_{on} should reduce in the presence of gold (using the available data on physical parameters of the Pi_2 toxin, the RD enhancement factor is approximately $\sim$10 at the $c = 2.5$ nM concentration; see Materials and methods). If we write the ratio of the 2D diffusion constant close to or in the gold island relative to that in the absence of gold (or at an infinitely long distance from the gold island) as a product of factors H and S, where H accounts for hydrodynamic effects and S for steric exclusion (tortuosity) effects, the resulting expression is (Phillips 2000):

$$D_2/D_{2,\infty} = H(\lambda, \phi) S(\lambda, \phi) \quad \text{(A2)}$$

where both H and S are exponential functions of the negative power of the λ and ϕ quantities, where λ is the ratio of the radius of the toxin and that of the gold bead and ϕ is the volume fraction excluded by the gold beads in the gold island. At small ϕ volume fractions, expanding the exponentials in a power series, $D_2/D_{2,\infty}$ can be approximated by the following formula:

$$D_2/D_{2,\infty} \approx 1 - F(\lambda)\phi \quad \text{(A3)}$$

where the $F(\lambda)$ term is a constant, determined by the toxin size/gold size ratio. If the gold island is modeled by an "equivalent cylinder" of radius R and height h, then the local excluded volume ϕ can be calculated as follows:

$$\begin{aligned} \phi &= \text{volume of beads in the cylinder / volume of cylinder} \\ &= (N \times 4r^3\pi/3)/(R^2\pi h) \end{aligned} \quad \text{(A4)}$$

where N is the number of gold beads in the island and r is the radius of a gold bead. This expression can be rearranged to the following form, by introducing the interparticle separation d and local surface density $\rho = 1/d^2$ of gold beads in the island:

$$\begin{aligned} \phi &= (4/3)(r/h)(r^2\pi)\rho \\ &= (4\pi/3)(r/h)(r/d)^2 \end{aligned} \quad \text{(A5)}$$

Although Eq. (A1) contains physical constants which can only be approximated, Eqs. (10), (A1), and (A2) show that there exists a formal relationship between the measurable η value and the local surface density (or inter-particle separation) of the gold beads. We should add that besides hindering diffusion, even direct modification of k_{on} may also occur.

References

Altomonte M, Pucillo C, Maio M (1999) The overlooked "non-classical" functions of major histocompatibility complex (MHC) class II antigens in immune and nonimmune cells. J Cell Physiol 179:251–256

Axelrod D, Wang MD (1994) Reduction-of-dimensionality kinetics at reaction-limited cell surface receptors. Biophys J 66:588–600

Bacsó Z, Matkó J, Szöllősi J, Gáspár R Jr, Damjanovich S (1996) Changes in membrane potential of target cells promotes cytotoxic activity of effector T lymphocytes. Immunol Lett 51:175–180

Bacsó Z, Bene L, Damjanovich L, Damjanovich S (2002) IFN-γ rearranges membrane topography of MHC-I and ICAM-1 in colon carcinoma cells. Biochem Biophys Res Commun 290:635–640

Barnstable CJ, Bodmer WF, Brown G, Galfré G, Milstein C, Williams AF, Ziegler A (1978) Production of monoclonal

antibodies to group A erythrocytes, HLA and other human cell surface anigens – new tools for genetic analysis. Cell 14:9–20

Bene L, Balázs M, Matkó J, Möst J, Dierich MP, Szöllősi J, Damjanovich S (1994) Lateral organization of the ICAM-1 molecule at the surface of human lymphoblasts: a possible model for its co-distribution with the IL-2 receptor, class I and class II HLA molecules. Eur J Immunol 24:2115–2123

Bene L, Szöllősi J, Balázs M, Mátyus L, Gáspár R Jr, Ameloot M, Dale RE, Damjanovich S (1997) Major histocompatibility class I protein conformation altered by transmembrane potential changes. Cytometry 27:353–357

Berg HC, Purcell EM (1977) Physics of chemoreception. Biophys J 20:193–219

Bernasconi CF (1976) Relaxation times in single-step systems. In: Relaxation kinetics. Academic Press, New York, pp 11–19

Bock J, Szabó I, Gamper N, Adams C, Gulbins E (2003) Ceramide inhibits the potassium channel Kv1.3 by the formation of membrane platforms. Biochem Biophys Res Commun 305:890–897

Bowlby MR, Fadool DA, Holmes TC, Levitan IB (1997) Modulation of the Kv1.3 potassium channel by receptor tyrosine kinases. J Gen Physiol 110:601–610

Chandy KG, DeCoursey TE, Cahalan MD, McLaughlin C, Gupta S (1984) Voltage-gated potassium channels are required for human T lymphocyte activation. J Exp Med 160:369–385

Cheng PC, Dykstra ML, Mitchell RN, Pierce SK (1999) A role for lipid rafts in B cell antigen receptor signaling and antigen targeting. J Exp Med 190:1549–1560

Chung I, Schlichter LC (1997) Native Kv1.3 channels are upregulated by protein kinase C. J Membr Biol 156:73–85

Damjanovich S, Pieri C (1991) Electro-immunology: membrane potential, ion-channel activities and stimulatory signal transduction in human T lymphocytes from young and elderly. Ann NY Acad Sci 621:29–39

Damjanovich S, Pieri C, Trón L (1992a) Ion channel activity and transmembrane signalling in lymphocytes. Ann NY Acad Sci 605:205–210

Damjanovich S, Szöllősi J, Trón L (1992b) Transmembrane signalling in T cells. Immunol Today 13:A12–A15

Damjanovich S, Matkó J, Mátyus L, Szabó G Jr, Szöllősi J, Pieri JC, Farkas T, Gáspár R Jr (1998) Supramolecular receptor structures in the plasma membrane of lymphocytes revealed by flow cytometric energy transfer, scanning force- and transmission electron-microscopic analyses. Cytometry 33:225–233

Damjanovich S, Bene L, Matkó J, Mátyus L, Krasznai Z, Szabó G Jr, Pieri C, Gáspár R Jr, Szöllősi J (1999) Two-dimensional receptor patterns in the plasma membrane of cells. A critical evaluation of their identification, origin and information content. Biophys Chem 82:99–108

De Petris S (1978) Immunoelectron microscopy and immunofluorescence in membrane biology. In: Korn ED (ed) Methods in membrane biology, vol 9. Plenum Press, New York, pp 1–201

DiSanto JP (1997) Cytokines: shared receptors, distinct functions. Curr Biol 7:R424–R426

Drénou B, Blancheteau V, Burgess DH, Fauchet R, Charron DJ, Mooney NA (1999) A caspase-independent pathway of MHC class II antigen-mediated apoptosis of human B lymphocytes. J Immunol 163:4115–4124

Edidin M, Wei T (1982) Lateral diffusion of H-2 antigens on mouse fibroblasts. J Cell Biol 95:458–462

Gáspár R Jr, Bene L, Damjanovich S, Muñoz-Garay C, Calderon-Aranda ES, Possani LD (1995). β-Scorpion toxin 2 from *Centruroides noxius* blocks voltage-gated K channels in human lymphocytes. Biochem Biophys Res Commun 213:419–423

Giurisato E, McIntosh DP, Tassi M, Gamberucci A, Benedetti A (2003) T cell receptor can be recruited to a subset of plasma membrane rafts, independently of cell signaling and attendantly to raft clustering. J Biol Chem 278:6771–6778

Goldstein SAN, Miller C (1993) Mechanism of charybdotoxin block of a voltage-gated K^+ channel. Biophys J 65:1613–1619

Hajdú P, Varga Z, Pieri C, Panyi G, Gáspár R Jr (2003) Cholesterol modifies the gating of Kv1.3 in human T lymphocytes. Eur J Physiol 445:674–682

Han J, Herzfeld J (1993) Macromolecular diffusion in crowded solutions. Biophys J 65:1155–1161

Haugh JM (2002) A unified model for signal transduction reactions in cellular membranes. Biophys J 82:591–604

Haugh JM, Lauffenburger DA (1997) Physical modulation of intracellular signaling processes by locational regulation. Biophys J 72:2014–2031

Hille B (1992) Ion channels of excitable membranes. Sinauer, Sunderland, Mass., USA

Holmes T, Berman CK, Swartz JE, Dagan D, Levitan IB (1997) Expression of voltage-gated potassium channels decreases cellular protein tyrosine phosphorylation. J Neurosci 17:8964–8974

Hori T, Uchiyama T, Tsudo M, Umadome H, Ohno H, Fukuhara S, Kita K, Uchino H (1987) Establishment of an interleukin 2-dependent human T cell line from a patient with T cell chronic lymphocytic leukemia who is not infected with human T cell leukemia/lymphoma virus. Blood 70:1069–1073

Huby RDJ, Dearman RJ, Kimber I (1999) Intracellular phosphotyrosine induction by major histocompatibility complex class II requires co-aggregation with membrane rafts. J Biol Chem 274:22591–22596

Janes PW, Ley SC, Magee AI (1999) Aggregation of lipid rafts accompanies signaling via the T cell antigen receptor. J Cell Biol 147:447–461

Jenei A, Varga S, Bene L, Mátyus L, Bodnár A, Bacsó Zs, Pieri C, Gáspár R Jr, Farkas T, Damjanovich S (1997) HLA class I and II antigenes are partially coclustered in the plasma membrane of human lymphoblastoid cells. Proc Natl Acad Sci USA 94:7269–7274

Jensen BS, Ødum N, Jørgensen NK, Christophersen P, Olesen S-P (1999) Inhibition of T cell proliferation by selective block of Ca^{2+}-activated K^+ channels. Proc Natl Acad Sci USA 96:10917–10921

Jürgens L, Nichtl A, Werner U (1999) Electron density imaging of protein films on gold-particle surfaces with transmission electron microscopy. Cytometry 37:87–92

Khodolenko BN, Hoek JB, Westerhoff HV (2000) Why cytoplasmic signalling proteins should be recruited to cell membranes. Trends Cell Biol 10:173–178

Kiss E, Balázs Cs, Bene L, Damjanovich S, Matkó J (1997) Effect of TSH and anti-TSH receptor antibodies on the plasma membrane potential of polymorphonuclear granulocytes. Immunol Lett 55:173–177

Koo GC, Blake JT, Talento A, Nguyen M, Lin S, Sirotina A, Shah K, Mulvany K, Hora D Jr, Cunningham P, Wunderler DL, McManus OB, Slaughter R, Bugianesi R, Felix J, Garcia M, Williamson J, Kaczorowski G, Sigal NH, Springer MS, Feeney W (1997) Blockade of the voltage-gated potassium channel $K_v1.3$ inhibits immune responses in vivo. J Immunol 158:5120–5128

Lampson LA, Levy R (1980) Two populations of Ia-like molecules on a human B cell line. J Immunol 125:293–299

Levite M (2001) Nervous immunity: neurotransmitters, extracellular K^+ and T-cell function. Trends Immunol 22:2–5

Levite M, Cahalon L, Peretz A, Hershkovicz R, Sobko A, Ariel A, Desai R, Attali B, Lider O (2000) Extracellular K^+ and opening of voltage-gated potassium channels activate T cell integrin function: physical and functional association between Kv1.3 channels and β_1 integrins. J Exp Med 191:1167–1176

Martel J, Dupuis G, Deschênes P, Payet MD (1998) The sensitivity of the human Kv1.3 (hKv1.3) lymphocyte K^+ channel to regulation by PKA and PKC is partially lost in HEK 293 host cells. J Membr Biol 161:183–196

Martens JR, Navarro-Polanco R, Coppock EA, Nishiyama A, Parshley L, Grobaski TD, Tamkun MM (2000) Differential targeting of Shaker-like potassium channels to lipid rafts. J Biol Chem 275:7443–7446

Matkó J, Edidin M (1997) Energy transfer methods for detecting molecular clusters on cell surfaces. Methods Enzymol 278:444–462

Matkó J, Bodnár A, Vereb G, Bene L, Vámosi G, Szentesi G, Szöllősi J, Hořejší V, Gáspár R Jr, Waldmann TA, Damjanovich S (2002) GPI-microdomains (membrane rafts) and signaling of the multi-chain interleukin-2 receptor in human lymphoma/leukemia T cell lines. Eur J Biochem 269:1199–1208

Mátyus L (1992) Fluorescence resonance energy transfer measurements on cell surfaces. A spectroscopic tool for determining protein interactions. J Photochem Photobiol B 12:323–337

Mátyus L, Pieri C, Recchioni R, Moroni F, Bene L, Trón L, Damjanovich S (1990) Voltage gating of Ca^{2+}-activated potassium channels in human lymphocytes. Biochem Biophys Res Commun 171:325–329

Mátyus L, Bene L, Heiligen H, Rausch J, Damjanovich S (1995) Distinct association of transferrin receptor with HLA class I molecules on HUT-102B and JY cells. Immunol Lett 44:203–208

Minton XXX (1992) Confinement as a determinant of macromolecular structure and reactivity. Biophys J 63:1090–1100

Murphy RM, Slayter H, Schurtenberger P, Chamberlin RA, Colton CK, Yarmush ML (1988) Size and structure of antigen-antibody complexes. Biophys J 54:45–56

Nagy P, Mátyus L, Jenei A, Panyi Gy, Varga S, Matkó J, Szöllősi J, Gáspár R Jr, Jovin TM, Damjanovich S (2001) Cell fusion experiments reveal distinctly different association characteristics of cell-surface receptors. J Cell Sci 144:4063–4071

Nelson BH, Willerford DM (1998) Biology of the interleukin-2 receptor. Adv Immunol 70:1–81

O'Connel KMS, Martens JR, Tamkun MM (2004) Localization of ion channels to lipid raft domains within the cardiovascular system. Trends Cardiovasc Med 14:37–42

Péter M Jr, Varga Z, Panyi G, Bene L, Damjanovich S, Pieri C, Possani LD, Gáspár R Jr (1998) *Pandinus imperator* scorpion venom blocks voltage-gated K^+ channels in human lymphocytes. Biochem Biophys Res Commun 242:621–625

Péter M Jr, Hajdu P, Varga Z, Damjanovich S, Possani LD, Panyi G, Gáspár R Jr (2000) Blockage of human T lymphocyte Kv1.3 channels by Pi1, a novel class of scorpion toxin. Biochem Biophys Res Commun 278:34–37

Péter M Jr, Varga Z, Hajdu P, Gáspár R Jr, Damjanovich S, Horjales E, Possani LD, Panyi G (2001) Effects of toxins Pi2 and Pi3 on human T lymphocyte Kv1.3 channels: the role of Glu7 and Lys24. J Membr Biol 179:13–25

Phillips RJ (2000) A hydrodynamic model for hindered diffusion of proteins and micelles in hydrogels. Biophys J 79:3350–3354

Pieri C, Bacsó Z, Recchioni R, Moroni F, Balázs M, Gáspár R Jr, Damjanovich S (1992) Bretylium differentiates between distinct signal transducing pathways in human lymphocytes. Biochem Biophys Res Commun 190:654–659

Schnitzer JE (1988) Analysis of steric partition behavior of molecules in membranes using statistical physics. Application to gel chromatography and electrophoresis. Biophys J 54:1065–1076

Schütz GJ, Hesse J, Freudenthaler G, Pastushenko VPh, Knaus H-G, Pragl B, Schindler H (2000a) 3D mapping of individual ion channels on living cells. Single Mol 1:153–157

Schütz GJ, Pastushenko VPh, Gruber HJ, Knaus H-G, Pragl B, Schindler H (2000b) 3D imaging of individual ion channels in live cells at 40 nm resolution. Single Mol 1:25–31

Simons K, Toomre D (2000) Lipid rafts and signal transduction. Nat Rev Mol Cell Biol 1:31–39

Skov S, Klausen P, Claesson MH (1997) Ligation of major histocompatibility complex (MHC) class I molecules on human T cells induces cell death through PI-3 kinase-induced c-Jun NH_2-terminal kinase activity: a novel apoptotic pathway distinct from Fas-induced apoptosis. J Cell Biol 139:1523–1531

Skov S, Nielsen M, Bregenholt S, Ødum N, Claesson MH (1998) Activation of Stat-3 is involved in the induction of apoptosis after ligation of major histocompatibility complex class I molecules on human Jurkat T cells. Blood 91:3566–3573

Spack EG Jr, Packard B, Wier ML, Edidin M (1986) Hydrophobic adsorption chromatography to reduce nonspecific staining by rhodamine-labeled antibodies. Anal Biochem 158:233–237

Su MW-C, Yu C-L, Burakoff SJ, Jin Y-J (2001) Targeting Src homology 2 domain-containing tyrosine phosphatase (SHP-1) into lipid rafts inhibits CD3-induced T cell activation. J Immunol 166:3975–3982

Szöllősi J, Damjanovich S, Balázs M, Nagy P, Trón L, Fulwyler MJ, Brodsky FM (1989) Physical association between MHC class I and class II molecules detected on the cell surface by flow cytometric energy transfer. J Immunol 143:208–213

Szöllősi J, Hořejší V, Bene L, Damjanovich S (1996) Supramolecular complexes of MHC class I, MHC class II, CD20 and tetraspan molecules (CD53, CD81, CD82) at the surface of a B cell line JY. J Immunol 157:2939–2946

Tanabe M, Sekimata M, Ferrone S, Takiguchi M (1992) Structural and functional analysis of monomorphic determinants recognized by monoclonal antibodies reacting with HLA class I alpha 3 domain. J Immunol 148:3202–3209

Tokita M, Miyoshi T, Takegoshi K, Hikichi K (1996) Probe diffusion in gels. Phys Rev E 53:1823–1827

Tomadakis MM, Sotirchos SV (1993) Transport properties of random arrays of freely overlapping cylinders with various orientation distributions. J Chem Phys 98:616–626

Tong J, Anderson JL (1996) Partitioning and diffusion of proteins and linear polymers in polyacrylamide gels. Biophys J 70:1505–1513

Trón L (1994) Experimental methods to measure fluorescence resonance energy transfer processes. In: Damjanovich S, Szöllősi J, Trón L, Edidin M (eds) Mobility and proximity in biological membranes. CRC, Boca Raton, Fla., USA, pp 1–47

Trón L, Szöllősi J, Damjanovich S, Helliwell SH, Arndt-Jovin DJ, Jovin TM (1984) Flow cytometric measurement of fluorescence resonance energy transfer on cell surfaces. Quantitative evaluation of the transfer efficiency on a cell-by-cell basis. Biophys J 45:939–946

Tsong TY, Astumian RD (1987) Electroconformational coupling and membrane protein function. Prog Biophys Mol Biol 50:1–20

Van Der Meer BW, Coker G III, Chen S-YS (1994) Resonance energy transfer, theory and data. VCH, Weinheim, Germany, p 155

Vereb G, Matkó J, Vámosi G, Ibrahim SM, Magyar E, Varga S, Szöllősi J, Jenei A, Gáspár R Jr, Waldmann TA, Damjanovich S (2000) Cholesterol-dependent clustering of IL-2Rα and its colocalization with HLA and CD48 on T lymphoma cells suggest their functional association with lipid rafts. Proc Natl Acad Sci USA 97:6013–6018

Vereb G, Szöllősi J, Matkó J, Nagy P, Farkas T, Vígh L, Mátyus L, Waldmann TA, Damjanovich S (2003) Dynamic, yet structured: the cell membrane three decades after the Singer-Nicolson model. Proc Natl Acad Sci USA 100:8053–8058

Wade WF, Davoust J, Salamero J, André P, Watts TH, Cambier JC (1993) Structural compartmentalization of MHC class II signaling function. Immunol Today 14:539–546

Wang D, Gou S-Y, Axelrod D (1992) Reaction rate enhancement by surface diffusion of adsorbates. Biophys Chem 43:117–137